Higher-Order Cumulants of Net-Proton Multiplicity Distributions in $^{96}_{40}$Zr+$^{96}_{40}$Zr and $^{96}_{44}$Ru+$^{96}_{44}$Ru Collisions at $\sqrt{s_{\mathrm{NN}}} = 200$ GeV*

Ho San Ko (for the STAR Collaboration)†

Lawrence Berkeley National Laboratory

Received July 30, 2022

The Relativistic Heavy Ion Collider (RHIC) at Brookhaven is a facility to create and study the strongly interacting Quark-Gluon Plasma (QGP). Higher-order cumulants of the conserved quantities and their ratios are powerful tools to study the properties of QGP and explore the QCD phase structure, such as critical point and/or the first-order phase transition boundary. In these proceedings, we present the net-proton cumulants and their ratios up to sixth-order as a function of multiplicity using high statistics data of $^{96}_{40}$Zr+$^{96}_{40}$Zr and $^{96}_{44}$Ru+$^{96}_{44}$Ru collisions at $\sqrt{s_{\mathrm{NN}}} = 200\,\mathrm{GeV}$. The STAR experiment collected two billion events for each colliding system. We compared the multiplicity dependence to the published net-proton cumulants in Au+Au collisions at $\sqrt{s_{\mathrm{NN}}} = 200\,\mathrm{GeV}$. In addition, we compared the results to Lattice QCD, the Hadron Resonance Gas model, and hadronic transport model calculations. The physics implications are discussed.

1. Introduction

Lattice QCD calculations show that the phase transition between the QGP state and the hadronic state is an analytic crossover at vanishing baryonic chemical potential (μ_B) [1] and at the temperature of 156.5 ± 1.5 MeV [2]. QCD based model calculations, see Ref. [3] for example, predict a critical point followed by a first-order phase transition at high μ_B. STAR detector at RHIC searches for the possible signature of the critical point and the first-order phase transition in the QCD phase diagram on temperature and μ_B plane QCD phase diagram by scanning the collision energy [4, 5].

Fluctuations of conserved quantities such as, net-baryon number, is used for the critical point search. Moment analyses of these event-by-event fluctu-

* Quark Matter 2022

† h-s.ko@lbl.gov

ating quantities are performed by studying their cumulants. The definitions of cumulants are in Sec. 2. Experimentally, the net-proton number is used as a proxy for the net-baryon number [6, 7].

It is expected that the fourth-order cumulant has a non-monotonic energy dependence in the vicinity of the critical point [8, 9, 10, 11]. Fourth-order cumulant (C_4/C_2) analysis of net-proton in Au+Au collisions at STAR shows a non-monotonic energy dependence at $\sqrt{s_{\mathrm{NN}}} = 7.7$ - 62.4 GeV with a significance of 3.1σ [5, 12]. Recent analyses of Au+Au collisions at $\sqrt{s_{\mathrm{NN}}} = 2.4$ and 3 GeV, at HADES [13] and STAR [14] respectively, show a suppression of net-proton C_4/C_2. The hadronic transport model, UrQMD [15], reproduces the data at $\sqrt{s_{\mathrm{NN}}} = 3$ GeV. Comparing to the transport model and the higher energy results, the suppression of C_4/C_2 indicates that it is hadronic interaction dominant in this high baryon density region ($\mu_B \geq 750$ MeV). These results imply that if the critical point is created in heavy-ion collisions, it could only exist above the collision energy of 3 GeV [14].

Moving on to the low baryon density region, Lattice QCD calculations of crossover between QGP and hadronic phases predict the fifth and the sixth-order cumulants (C_5/C_1 and C_6/C_2) of the net-baryon number to be negative at the collision energy of $\sqrt{s_{\mathrm{NN}}} = 200$ GeV [16]. The C_6/C_2 of net-proton number at the same collision energy of Au+Au collisions was also measured at STAR [17, 18]. The result shows a systematic trend where the value decreases to be negative as the collision centrality moves from peripheral to central collisions. Then at the most central collisions, it becomes consistent with the Lattice QCD results in Ref. [16]. On the other hand, in two other collision energies, $\sqrt{s_{\mathrm{NN}}} = 27$ and 54.4 GeV, the results are consistent with zero.

STAR at RHIC collected 2 billion and 1.9 billion events for ${}^{96}_{40}\mathrm{Zr}+{}^{96}_{40}\mathrm{Zr}$ and ${}^{96}_{44}\mathrm{Ru}+{}^{96}_{44}\mathrm{Ru}$ collisions, respectively at $\sqrt{s_{\mathrm{NN}}} = 200$ GeV in 2018. Studying the net-proton cumulants and their ratios provide much improved statistics over Au+Au collision results. Additionally, in these proceedings, we inspect the collision system dependence by comparing the results from p+p , the isobars (${}^{96}_{40}\mathrm{Zr}+{}^{96}_{40}\mathrm{Zr}$ and ${}^{96}_{44}\mathrm{Ru}+{}^{96}_{44}\mathrm{Ru}$), and Au+Au at the same collision energy of $\sqrt{s_{\mathrm{NN}}} = 200$ GeV.

As mentioned later in the outlook of Sec. 5, analysis on cumulant ratios of mixed quantum numbers may enable us to measure the magnetic field created in the heavy-ion collisions [19]. Aside from the high statistics, the isobar collisions make them suitable data sets for this future analysis due to the charge number difference. Thus, checking the collision system dependence of the net-proton cumulants and ratios is needed before we move on to the next endeavor.

2. Experimental Observables

Cumulants from the first to the sixth-order can be written as:

$$\begin{aligned}
C_1 &= \langle N \rangle, \\
C_2 &= \langle (\delta N)^2 \rangle, \\
C_3 &= \langle (\delta N)^3 \rangle, \\
C_4 &= \langle (\delta N)^4 \rangle - 3\langle (\delta N)^2 \rangle^2, \\
C_5 &= \langle (\delta N)^5 \rangle - 10\langle (\delta N)^2 \rangle \langle (\delta N)^3 \rangle, \\
C_6 &= \langle (\delta N)^6 \rangle + 30\langle (\delta N)^2 \rangle^3 - 15\langle (\delta N)^2 \rangle \langle (\delta N)^4 \rangle - 10\langle (\delta N)^3 \rangle^2,
\end{aligned} \tag{1}$$

where N represents the event-by-event conserved quantity distribution and $\delta N = N - \langle N \rangle$. The symbol $\langle N \rangle$ represents the average value of N over the events. The higher the cumulant order, the more the cumulant is sensitive to the correlation length [20]. Taking the ratio of the cumulants cancels out the volume dependence and the ratios can be directly compared to theoretical calculations.

3. Analysis Setup

The (anti-)proton acceptance for the analysis is $0.4 < p_T < 2.0$ GeV/c in transverse momentum and $|y| < 0.5$ in rapidity. The events are categorized into nine different collision centralities: 0-5%, 5-10%, 10-20%, 20-30%,...,70-80%. The collision centralities are determined by the number of charged particle multiplicity. In this analysis, the charged particle multiplicity is defined as the number of detected charged particles excluding the (anti-) proton tracks in the pseudorapidity region of $|\eta| < 1$.

The efficiencies of the detector acceptance and tracking are corrected track-by-track [21, 22]. The Centrality Bin Width Correction (CBWC) is applied when merging the multiplicity bins into centrality bins [23]. The statistical uncertainties are calculated based on the Delta theorem [24].

4. Results

The net-proton cumulants up to sixth-order are plotted in Fig. 1. Results in Au+Au collisions [12] are also plotted for comparison. The detectors efficiencies for all data points are corrected. The results are plotted to the average number of participating nucleons ($\langle \mathrm{N_{part}} \rangle$). Results in $^{96}_{40}$Zr+$^{96}_{40}$Zr and $^{96}_{44}$Ru+$^{96}_{44}$Ru are consistent. In addition, both results from isobars and Au+Au at $\sqrt{s_{\mathrm{NN}}} = 200$ GeV GeV follow the same $\langle \mathrm{N_{part}} \rangle$ trend. As shown in Fig. 1, the data are compared with the UrQMD calculations, where the same acceptance as used in STAR analysis was adopted. The

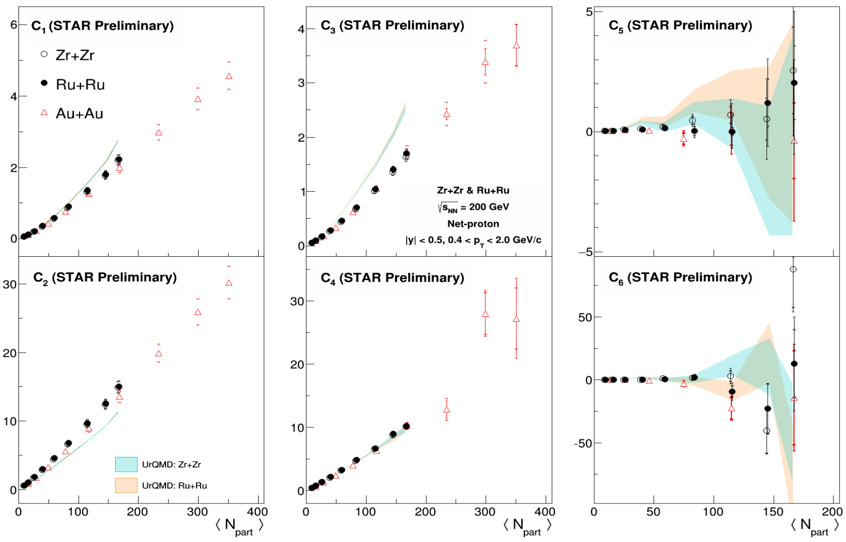

Fig. 1: Cumulants of net-proton in ${}^{96}_{40}$Zr+${}^{96}_{40}$Zr and ${}^{96}_{44}$Ru+${}^{96}_{44}$Ru collisions from the first to the sixth-order are plotted to the average number of participating nucleons. Results from Au+Au collisions are presented for comparison. The x-axis ranges for C_5 and C_6 are decreased. Detector efficiencies are corrected. The bars and brackets for each marker represent the statistical and systematic uncertainties, respectively. UrQMD calculations are shown in bands.

UrQMD generally shows a similar trend as in the data, however overpredicts C_1 and C_3 while it underpredicts C_2.

Figure 2 compares the higher-order cumulant ratios C_4/C_2, C_5/C_1, and C_6/C_2 at $\sqrt{s_{\mathrm{NN}}} = 200$ GeV for different collision systems, p+p, the isobars, and Au+Au [12, 17], as a function of charged particle multiplicity. For better statistics, the collision centralities from 0% to 40% are merged into one central collision bin. For p+p collisions, only the cumulant ratio in average charged particle multiplicity bin is shown. Not only the ${}^{96}_{40}$Zr+${}^{96}_{40}$Zr and the ${}^{96}_{44}$Ru+${}^{96}_{44}$Ru results are consistent, but all results from different collision systems agree among themselves. All cumulant ratios in Fig. 2 decrease as the multiplicity increases and deviate further from the Hadron Resonance Gas (HRG) model calculations in the Grand Canonical Ensemble picture. Although the UrQMD calculations describe the overall multiplicity dependent trend, they overpredict the presented higher-order ratios. At the top 0-40% central Au+Au collisions, the results become consistent with the Lattice QCD prediction for the formation of thermalized QCD matter and smooth crossover transition. PYTHIA 8.2 (Pythia) calculations in Fig. 2 represent the cumulant ratios averaged over charged particle multiplicity of

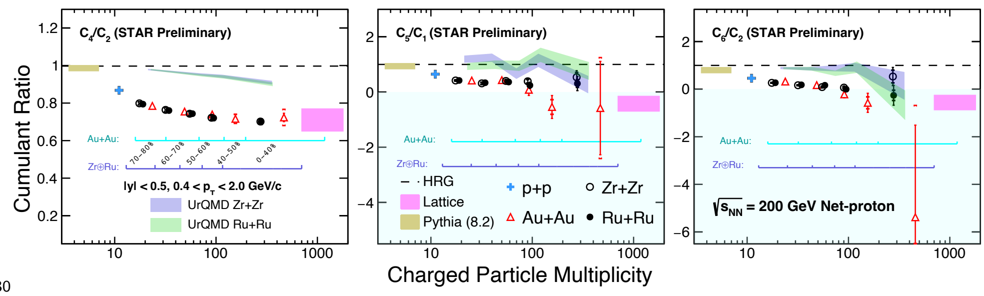

Fig. 2: Cumulant ratios C_4/C_2, C_5/C_1, and C_6/C_2 of ${}^{96}_{40}$Zr+${}^{96}_{40}$Zr and ${}^{96}_{44}$Ru+${}^{96}_{44}$Ru collisions as a function of charged particle multiplicity. Results from Au+Au and p+p collisions are presented for comparison. Cumulant ratios for p+p presented only in averaged charged particle multiplicity. The detector efficiencies for the charged particle multiplicity are not corrected but corrected for the cumulant ratios. The bars and brackets for each marker represent the statistical and systematic uncertainties, respectively. UrQMD calculations are shown in bands. HRG calculations are shown in dashed lines. Magenta bands represent Lattice QCD prediction for the formation of thermalized QCD matter. Pythia calculations shown in gold bands are for average charged particle multiplicity in p+p collisions.

the p+p collisions. All the higher-order cumulant ratios from Pythia are consistently positive which is inconsistent with the Lattice QCD results in the case of the fifth and the sixth-order.

5. Summary and Outlook

We have presented net-proton cumulants and their ratios up to sixth-order in isobar collisions at $\sqrt{s_{\rm NN}}$ = 200 GeV. The results fit into the multiplicity dependence of cumulant ratios in p+p and Au+Au collisions. Although the hadronic transport model, UrQMD, over- and underpredicts the results, it shows a similar trend as in the data. All C_4/C_2, C_5/C_1, and C_6/C_2 show decreasing trends as multiplicity increases and deviate further from the HRG model calculation. In the most central collision centrality of Au+Au collisions, the higher-order cumulant ratios become consistent with the Lattice QCD calculations. The consistency between the data and the theory calculations implies that the transition between the thermalized QGP to the hadronic matter is a smooth crossover in central Au+Au collisions at top RHIC energy. This is a direct comparison between data and the first principle QCD calculations.

Other than the fluctuation measurements, one of the most important studies in the field of heavy-ion collisions is Chiral Magnetic Effect (CME). Measuring the magnetic field created in the heavy-ion collisions would greatly help to study the CME. Recent Lattice QCD results show a possibility to experimentally assess the magnetic field created in the heavy-ion collisions by studying the cumulant ratios of mixed quantum numbers [19]. Due to the charge number difference between ${}^{96}_{40}$Zr+${}^{96}_{40}$Zr and ${}^{96}_{44}$Ru+${}^{96}_{44}$Ru, we expect about a 15% difference in the magnetic field squared [25]. Therefore, the high statistics of ${}^{96}_{40}$Zr+${}^{96}_{40}$Zr and ${}^{96}_{44}$Ru+${}^{96}_{44}$Ru collision data collected by STAR offer an opportunity to measure the magnetic field strength, or at least, the difference between the isobars.

References

[1] Y. Aoki *et al. Nature* 443 (2006), pp. 675–678.

[2] A. Bazavov *et al.*, HotQCD. *Phys. Lett. B* 795 (2019), pp. 15–21.

[3] M. A. Halasz *et al. Phys. Rev. D* 58 (1998), p. 096007.

[4] L. Adamczyk *et al.*, STAR. *Phys. Rev. C* 96.4 (2017), p. 044904.

[5] J. Adam *et al.*, STAR. *Phys. Rev. Lett.* 126.9 (2021), p. 092301.

[6] Y. Hatta and M. A. Stephanov. *Phys. Rev. Lett.* 91 (2003). [Erratum: Phys.Rev.Lett. 91, 129901 (2003)], p. 102003.

[7] M. Kitazawa and M. Asakawa. *Phys. Rev. C* 86 (2012). [Erratum: Phys.Rev.C 86, 069902 (2012)], p. 024904.

[8] M. A. Stephanov. *Phys. Rev. Lett.* 107 (2011), p. 052301.

[9] B. J. Schaefer and M. Wagner. *Phys. Rev. D* 85 (2012), p. 034027.

[10] J.-W. Chen *et al. Phys. Rev. D* 93.3 (2016), p. 034037.

[11] J.-W. Chen *et al. Phys. Rev. D* 95.1 (2017), p. 014038.

[12] M. S. Abdallah *et al.*, STAR. *Phys. Rev. C* 104.2 (2021), p. 024902.

[13] J. Adamczewski-Musch *et al.*, HADES. *Phys. Rev. C* 102.2 (2020), p. 024914.

[14] M. S. Abdallah *et al.*, STAR. *Phys. Rev. Lett.* 128.20 (2022), p. 202303.

[15] M. Bleicher *et al. J. Phys. G* 25 (1999), pp. 1859–1896.

[16] A. Bazavov *et al. Phys. Rev. D* 101.7 (2020), p. 074502.

[17] M. S. Abdallah *et al.*, STAR. *Phys. Rev. Lett.* 127.26 (2021), p. 262301.

[18] STAR. arXiv: `2207.09837v1 [nucl-ex]`.

[19] H. -T. Ding *et al. Eur. Phys. J. A* 57.6 (2021), p. 202.

[20] M. A. Stephanov. *Phys. Rev. Lett.* 102 (2009), p. 032301.

[21] T. Nonaka, M. Kitazawa, and S. Esumi. *Phys. Rev. C* 95.6 (2017). [Erratum: Phys.Rev.C 103, 029901 (2021)], p. 064912.

[22] X. Luo and T. Nonaka. *Phys. Rev. C* 99.4 (2019), p. 044917.

[23] X. Luo *et al. J. Phys. G* 40 (2013), p. 105104.

[24] X. Luo. *J. Phys. G* 39 (2012), p. 025008.

[25] M. S. Abdallah *et al.*, STAR. *Phys. Rev. C* 105.1 (2022), p. 014901.